Chemical Engineering Journal 390 (2020) 124647

Contents lists available at ScienceDirect

Chemical Engineering Journal

journal homepage: www.elsevier.com/locate/cej

Insights into the interaction of iodide and iodine with Cu(II)-loaded bispicolylamine chelating resin and applications for nuclear waste treatment

Thomas J. Robshaw[a,*], Sion M. Griffiths[a], Adam Canner[a], James P. Bezzina[a], Archibald G.L. Waller[a], Deborah B. Hammond[b], Sandra van Meurs[b], Mark D. Ogden[a]

[a] Separations and Nuclear Chemical Engineering Research, Department of Chemical and Biological Engineering, Sir Robert Hadfield Building, University of Sheffield, S1 3JD, UK
[b] Department of Chemistry, Dainton Building, University of Sheffield, S3 7HF, UK

HIGHLIGHTS

- A novel use for a copper-functionalised chelating resin is demonstrated.
- High capacity and selectivity for iodide, in static and dynamic experiments, is proven.
- Uptake proceeds via ligand-exchange, REDOX chemistry and charge-transfer complex formation.
- A fraction of the bound iodide is extremely chemically and thermally stable.
- The adsorbent shows potential for the treatment of spent nuclear fuel reprocessing waste.

GRAPHICAL ABSTRACT

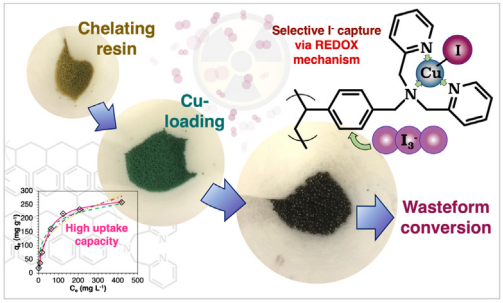

ARTICLE INFO

Keywords:
Radioiodine
Metal-loaded resin
Bispicolylamine
Spent nuclear fuel
Ion-exchange
Adsorption

ABSTRACT

Radioiodine is a challenging contaminant to remove from aqueous wastestreams, resulting from spent nuclear fuel reprocessing. To create a selective, economical adsorbent, a Cu-loaded bispicolylamine chelating resin was produced, from commercially available reagents and its performance for removal of aqueous iodide and iodine was assessed. The resin possessed a large equilibrium uptake capacity of 305 ± 14 mg.g^{-1} iodide and 2940 ± 180 mg.g^{-1} total iodine. Performance was close to maximal over a pH range of 2–10. Capacity was reduced by ~55% by the addition of cocontaminants nitrate and molybdate, but resistance to suppression was greatly superior to non-modified polyamine resins, clearly seen in dynamic column experiments. The uptake mechanism was investigated spectroscopically and was found to proceed via ligand-exchange, with some in-situ REDOX chemistry occurring, resulting in the formation of Cu(I) and triiodide. The latter was concurrently adsorbed on to the resin and occupied both strong (Cu-associated) and weak (charge-transfer complex formation) binding sites. Thermal decomposition of the loaded resins revealed that the captured iodine was volatised at several different temperatures, according to strength of adsorption, but a large fraction was converted to stable CuI, suggesting a possible pathway towards volume-reduction and immobilisation as a final wasteform.

* Corresponding author.
E-mail address: tjrobshaw1@sheffield.ac.uk (T.J. Robshaw).

https://doi.org/10.1016/j.cej.2020.124647
Received 8 January 2020; Received in revised form 2 March 2020; Accepted 3 March 2020
Available online 05 March 2020
1385-8947/

1. Introduction

Ever-increasing global energy demand has led to a proliferation of commercial nuclear power stations. There are currently ~450 operating nuclear power reactors, with a further 60 under construction, supplying ~11% of the world's electricity [1]. Appropriate waste management is key to addressing inherent nuclear safety issues and one key challenge within this remit is the immobilisation of fission products from the nuclear fuel reprocessing cycle, to prevent release to the environment. Volatile gaseous fission products include ^{3}H, ^{85}Kr, ^{131}I and ^{129}I, with the two radioiodine species being of particular interest. ^{131}I decays rapidly ($t_{1/2}$ = 8 days) and with highly ionising radiation, with β-particles of energy 606 keV and γ-rays of energy 364 keV. It is thus not a radiation hazard in terms of waste disposal, but dangerous in the event of accidental release to the environment [2]. ^{129}I is less ionising, with β-particles of energy ≤ 154 keV and γ-rays of energy 39.6 keV, but is an extremely long-lived isotope ($t_{1/2}$ = 1.57 × 10^{7} years). All iodine species bioaccumulate rapidly and are stored by humans and animals in the thyroid gland. Indeed, radioiodine has been implicated in sudden rises in cases of thyroid cancer in children [3].

Spent nuclear fuel (SNF) reprocessing involves dissolution of the exhausted rods in HNO_3. This process, causes the volatilisation of ~98% of the iodine present in the waste, which then enters the plant off-gas system [4]. The residual aqueous iodine remaining in the raffinate is challenging to remove economically, the liquid having low pH and elevated levels of cocontaminants nitrate, and in particular, molybdate, which does not volatise to the same degree as iodine species [5]. There is no agreed industrial "best practice" for its treatment. The gaseous fraction is commonly captured by caustic scrubbing and this liquid stream is ultimately released to the ocean, within allowable discharge limits. However, as a result of this practice, ^{131}I is consistently accumulating in the marine ecosystem [6] and an arguably superior strategy is immobilisation within a solid matrix of low volume [7], followed by long-term geological disposal.

Solid-phase extractants have been investigated for the remediation of radioiodine. Activated carbon is the most common matrix and is used at an industrial scale, but requires impregnation by KI, triethylenediamine or NaOH to be effective [8,9]. Microporous organic polymers have been trialled for this purpose. These have very high adsorption capacity (> 3g.g^{-1}), but their large-scale synthesis is unrealistic, because of high cost of monomers and catalysts [10,11]. A small number of studies have focussed on commercial anion-exchange resins, which outperform activated carbon in terms of capacity, when the iodine in solution is present mainly in the form of iodide anions [12], which indeed is the case in the industrial raffinate [13]. The key issue however, is competition for binding sites, from the presence of both harder (NO_3^-) and softer (MoO_4^{2-}) bases at high concentrations. Our research group evaluated two weak base anion (WBA) resins for this purpose, Lewatit® A365 and Purolite® MTS9850, which demonstrated very high maximal iodide uptakes of 589 and 761 mg.g^{-1} respectively [14]. However, the polyamine functionalities were unselective towards the iodide anions, with both nitrate and molybdate causing significant suppression of uptake.

One strategy to create selective anion uptake is to use metal-loaded or -impregnated adsorbents, which utilise hard-soft-acid-base (HSAB) theory to target a certain species in a mixed waste-stream. For radioiodide removal, sorbent activation by silver is popular (AgI K_{sp} = 8.52 × 10^{-17}). La Hague nuclear reprocessing facility in France uses a silver-impregnated zeolite filter system [15] and Tokai in Japan employs alumina, dosed with $AgNO_3$ [16]. Other silver-loaded materials include mordenites [17] and commercial cation-exchange resins [18]. Although these materials are selective, their iodide uptake capacities are surprisingly poor, being mostly < 200 mg.g^{-1}. Some require careful storage to prevent in-situ Ag reduction and can also suffer from Ag leaching [18].

A more attractive metal for selective iodide capture may be copper, which has lesser, but still high affinity for iodide (CuI K_{sp} = 1.10 × 10^{-12}), lower molecular weight and is more economical. Research into Cu-loaded materials for iodide capture is very rare, being limited to activated carbon, modified with Cu nanoparticles [13].

Key considerations in the design of metal-loaded extractants are not only the affinity of the metal centres for the target anions, but the interaction between the metal and the extractant functionality. If this is too weak, the system can suffer from inorganic salt precipitation, which is problematic for dynamic water treatment systems [19]. To this point, it is well-established that Cu^{2+} has remarkable binding stability with the bispicolylamine (BPA) functionality over a wide pH range [20–22]. The metal ion binds to the neutral ligand with distorted square pyramidal geometry, allowing the exchange of two anionic ligands [23], therefore having high theoretical iodide capacity. It has even been shown that a Cu-loaded BPA ion-exchange resin can be repurposed to target alternative contaminants, namely tartaric acid [24]. However, the synergy of BPA functionality, Cu dosing and selective iodide capture has not been presented. Furthermore, the mechanistic understanding of this uptake process is very much incomplete, with no relevant literature found beyond the early work of Sutton [25]. Collectively, this provides the impetus for the current work.

In this study, we create the Cu-loaded form of a chelating ion-exchange resin, DOWEX™ M4195 (Fig. 1), for which we build a full assessment of the adsorbent for iodide and iodine removal from SNF reprocessing waste. This considers speciation, competing anions, working pH range and conversion to final waste-form and concludes that Cu-loaded BPA materials are among the most promising yet investigated for this pressing industrial problem. A mechanistic uptake process, which accounts for the data attained, is also suggested for the first time.

2. Experimental

2.1. Chemical reagents

All metal salts were of analytical reagent grade, unless otherwise stated. All solvents were of HPLC grade. All materials were used without further purification. Salts were dissolved in deionised water of > 18 MΩ resistivity. $CuCl_2{\cdot}2H_2O$, NaI, $NaNO_3$ and $Na_2MoO_4{\cdot}2H_2O$ were supplied by Sigma Aldrich. NaOH, Na_2CO_3, HNO_3 (68%) and methanol were supplied by Fisher Scientific. Standard solutions for potentiometry and ion chromatography analysis were made by dissolving NaCl, NaI, $NaNO_3$ and $Na_2MoO_4{\cdot}2H_2O$ (Fisher Scientific, > 99.99%, trace metals grade) in deionised water. DOWEX™ M4195 bispicolylamine resin was supplied by Sigma Aldrich. Specification as supplied is shown in Table S1.

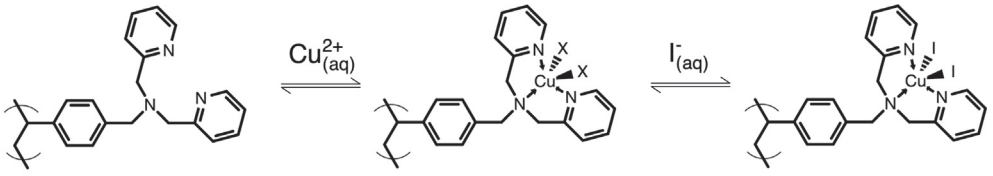

Fig. 1. Proposed metallation and iodide uptake of M4195 resin.

2.2. Preparation of M4195-Cu resin and other adsorption media

DOWEX™ M4195 is sold in partially-quaternised sulfate form, which gives optimal Cu-loading capabilities [26]. M4195 resin (2.00 g hydrated mass, as received) was contacted with a solution of $CuCl_2$ (100 mL, 100 mM) in a polypropylene bottle, which was agitated for 12 hr at room temperature. The resulting Cu-loaded resin (termed "M4195-Cu"), which took the form of turquoise beads, was washed with deionised water (2 L) and also stored in deionised water when not in use. The extent of Cu loading for M4195 was checked by analysis of the pre- and post-contact solution, using colorimetry (absorbance at 815 nm), with a VWR UV-6300PC spectrophotometer. The actual Cu concentration of M4195-Cu was determined by digestion of resin samples in $HNO_3/HClO_4$, followed by analysis with an Agilent 7500CE inductively-coupled mass spectrometer (ICP-MS).

For certain analyses, we also prepared the non-metallated version of M4195 (partially protonated) and the polyamine resin described in previous work, Purolite® MTS9850 [14]. This was achieved following the same procedure as before, with HNO_3 (1 M) as the contact solution.

2.3. M4195-Cu Iodide remediation experiments

M4195-Cu was handled in hydrated form. Iodide uptake capacity was calculated on a dry mass basis by determining the mass loss of the resin upon drying in an air-flow oven at 70 °C for a minimum of 24 hr. All uptake experiments were conducted at 20 °C. In a typical experiment, M4195-Cu (100 mg dry mass equivalent) was contacted with NaI solution (50 mL) in a polypropylene vial, which was agitated for 12 hr at room temperature on an orbital shaker (100 rpm). In pH-controlled experiments, samples were equilibrated to the desired pH, using NaOH and HNO_3 (0.001–1 M) over a 12 hr period, before being made up to final volume. For solutions of desired pH 2–11, proton concentration was checked using a standard AgCl electrode. For solutions of pH 0, 1, 12 and 13, the proton concentration, pre- and post-resin contact, was determined by titration against either standardised HCl or NaOH, using phenolphthalein indicator. In certain experiments, $NaNO_3$ and $Na_2MoO_4{\cdot}2H_2O$ were added as sources of the competing anions. In iodine mixed speciation solutions, iodine was added to NaI solutions in glass bottles and allowed to dissolve over a period of 48 hr on the orbital shaker (100 rpm).

In single-species experiments, the iodide concentration of pre- and post-resin-contact solutions was determined using a Cole-Parmer ion-selective electrode (ISE) and the uptake at equilibrium (q_e) in $mg.g^{-1}$ was determined by mass balancing. All samples contained 2% $NaNO_3$ (5 M) as ionic strength adjustment buffer. In mixed iodine species studies, free I^- was again quantified via ISE and total iodine determined via ICP-MS. In competition studies, uptake of iodide, nitrate and molybdate, along with release of chloride, was simultaneously quantified via anion chromatography, using a Metrohm 883 Basic IC plus, with a Metrosep A Supp 5 150/4.0 column and $Na_2CO_3/NaHCO_3$ eluent.

2.4. Ion-exchange column simulations

In a typical dynamic experiment, M4195-Cu (5.76 g hydrated mass, 5.50 mL) was packed into a 6 mL polypropylene column, with porous frits above and below the resin bed. Inlet solutions were passed through the column in a reverse-flow system, using Watson Marlow Marprene® tubing (internal diameter 0.5 mm), connected to a Watson Marlow 120S peristaltic pump. The system was calibrated to deliver a flow rate of 1.0 bed volume.hr^{-1} (bed volume (BV) = equivalent volume of solution to that of the resin mass). 0.5 BV fractions were collected and analysed via ISE, as previously described.

2.5. Chemical analysis of resin

Samples of M4195-Cu and other adsorption media were isolated, at different processing stages, for various analytical techniques. Samples were washed of residual contact solution with 10 BV of deionised water and ground to a slurry with a mortar and pestle, then dried in an air-flow oven at 40 °C for > 24 hr prior to experimentation.

For elemental analysis (CHNS), analysed samples were catalytically combusted, using an Elementar Vario MICRO Cube. Gases were separated using a Thermal Programmed Desorption column and detected using a Thermal Conductivity Detector. Fourier transform infrared (FTIR) spectroscopy was performed using a Perkin-Elmer UATR2 and Spectrum 100. Nuclear magnetic resonance (NMR) spectroscopy was performed on samples, in the solid state, using 1D ^1H–^{13}C and ^1H-^{15}N cross-polarisation magic angle spinning (CP/MAS), with a Bruker Avance III HD 500 MHz spectrometer. Full operating parameters are shown in Supporting Information, p1. RAMAN spectroscopy was conducted using a Renishaw inVia RAMAN microscope, using a 514.5 nm laser, operating at 1% intensity. X-ray diffraction (XRD) analysis was performed using a Bruker D2 Phaser X-ray diffractometer, using dual Ni K-β filters. Diffractograms were matched using the International Center for Diffraction Data (ICDD) PDF-4 + database [27]. X-ray photoelectron spectroscopy (XPS) was carried out using a Kratos Supra spectrometer, with a monochromated Al source and two analysis points per sample. Again, operating parameters are shown in Supporting Information, p13. TGA traces were attained using a Perkin Elmer TGA 4000. Samples were weighed (5–25 mg) into a ceramic crucible and heated from ambient to 100 °C at a rate of 50 °C.min^{-1}, held at 100 °C for 10 min, then heated from 100 °C to 900 °C at 50 °C.min^{-1}. Combustion and partial combustion of spent resin samples was achieved using a Vecstar ashing furnace.

All error values were derived from 2 × the standard deviation over at least 2 replicate samples or measurements, then propagated as necessary.

3. Results and discussion

3.1. Cu-loading and elemental composition of resin

The adsorption of Cu by M4195 was verified as 91.0 ± 1.3 $mg.g^{-1}$ (1.43 ± 0.02 $mmol.g^{-1}$) by analysis of 5 replicate samples. The

Table 1
Elemental composition of M4195 resin at various process stages. Error values represent approximate 95% confidence intervals over 3 replicate samples.

Sample	Mass % (mmol.g^{-1})					
	C	H	N	S	Cl	Cu
M4195 as-received	69.1 ± 1.2 (57.6 ± 1.0)	6.17 ± 0.76(61.1 ± 7.5)	8.31 ± 0.21 (5.95 ± 0.15)	2.81 ± 0.79 (0.877 ± 0.25)	2.65 ± 0.54 (0.747 ± 0.15)	–
M4195 deprotonated	79.4 ± 0.5 (66.2 ± 0.4)	6.70 ± 0.11 (66.3 ± 1.1)	9.41 ± 0.14 (6.72 ± 0.10)	0.56 ± 0.23 (0.175 ± 0.071)	0.555 ± 0.16 (0.157 ± 0.044)	–
M4195-Cu	60.3 ± 0.2 (50.2 ± 0.1)	5.81 ± 0.04 (57.5 ± 0.4)	7.01 ± 0.04 (5.00 ± 0.03)	0.660 ± 0.20 (0.206 ± 0.062)	8.43 ± 0.13 (2.38 ± 0.04)	7.98 ± 0.15 (1.26 ± 0.02)

relative elemental mass percentages of M4195 and M4195-Cu are shown in Table 1. It can be seen that the concurrent adsorption of two chloride counterions with one Cu^{2+} ion leads to the Cu mass % in the resulting M4195-Cu material being rather lower in comparison. We also analysed a fully-deprotonated sample, achieved by equilibration with 1 M NaOH, for comparative purposes.

The atomic composition of M4195 as-received was similar to that previously reported [28]. Comparing the molar concentrations of N and adsorbed Cu suggested that the supposed binding interaction was not 100% as shown in Fig. 1. Indeed, it has been shown that Cu^{2+} ions can doubly-chelate to such resins by interaction with 2 BPA groups [29]. Grinstead stated that a fraction of aliphatic amines in M4195 are permanently quaternised (presumably methylated) and therefore cannot chelate [30]. This is supported by the elemental composition of the deprotonated sample (Table 1), which shows that some sulfate counteranions, associated with quarternary ammonium groups are still present after the 1 M NaOH treatment. This does not exclude the possibility that a Cu^{2+} ion could interact with the picolyl nitrogens of the ligand only, although Spencer *el al.* postulated that doubly-chelated Cu would interact with all 6 nitrogens [29]. Nonetheless, it is possible that not every resin-bound BPA group is accessible to Cu^{2+} ions. The Cu capacity was above that observed by Kolodynska *et al.* (50 $mg.g^{-1}$, chloride media) [28], which was however determined with $[Cu^{2+}]$ an order of magnitude lower. Grinstead originally quoted a capacity for M4195 of 40 $g.L^{-1}$, using a similar loading procedure to our own [30] which, if assumed to be wet settled volume, equates to ~120 $mg.g^{-1}$ (conversion determined by our own mass loss upon drying experiments). This was determined in sulfate media and Kolodynska *et al.* did find that choice of Cu counteranion was influential to uptake capacity, reporting ~14% higher Cu uptake capacity for M4195 in sulfate media, rather than chloride [28]. Assuming that every S atom represents a divalent sulfate ion, ~1/3 of N atoms present in the partially-hydrated samples, as received, would have been protonated. The pK_as for a resin-bound BPA functionality have been investigated, with pK_1 expected at 0.50–1.6, pK_2 at 2.1–2.7 and pK_3 at 3.4–4.1 [22,31,32]. The pH of a suspension of M4195 in deionised water was 1.97, so the implied degree of protonation cannot be explained by the presence of sulfate only. We performed anion chromatography analysis on a sample of the separated water (results not shown), which revealed that the observed Cl content was in the form of chloride ions and hence that this is the other major counteranion involved in the production of M4195.

3.2. Iodide removal as a function of pH

Uptake of iodide by M4195-Cu over a pH range of 0–13 is shown in Fig. 2, which also shows simultaneous leaching of Cu. The resin possessed a broad operating range of pH 2–10, implying that M4195-Cu could be used for both direct remediation of SNF and iodide extraction from caustic scrubbing solution, with appropriate dilution.

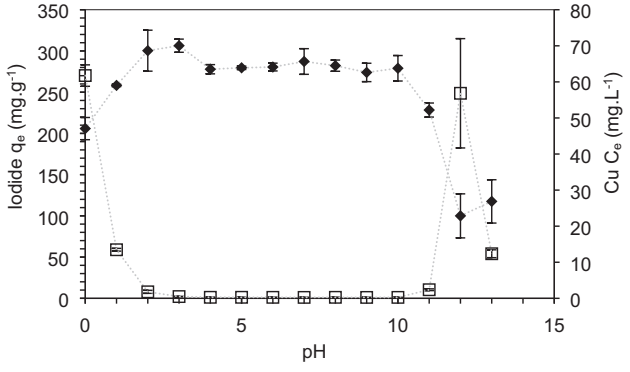

Fig. 2. Iodide uptake by M4195-Cu over pH range 0–13 with adjustments being made using HNO_3 and NaOH. ◆ = iodide uptake. □ = leaching of Cu into solution. Initial $[I^-]$ = 1.00 $g.L^{-1}$. Error bars represent approximate 95% confidence intervals derived from 2 × experimental reps.

As expected, Cu leaching was also negligible over the working pH range. There was however, loss of Cu in acidic conditions, starting at pH 2 and becoming significant at pH 1. Previous work, executed in sulfate media, has found the affinity of M4195 for Cu at pH 1 to be near maximal [21,30], suggesting that the stability of the BPA-Cu complex in nitrate media is lesser. These however, were uptake, rather than leaching experiments. It should also be noted that, as subsequent results will show, some reduction of the Cu^{2+} centres took place during the uptake process, which could well be promoted by excess acid. CuI solublises in NaI solutions to give the linear anion $[CuI_2]^-$. Therefore, this mechanism could also contribute to leaching behaviour. At pH 0, 66.5 ± 1.5% of the Cu originally loaded was calculated to remain on the resin. This closely correlates with the iodide uptake, which was 67.3 ± 4.4% of the observed maximum at pH 3. This demonstrates that the protonated amine groups, resulting from Cu desorption, are non-selective towards iodide, which is out-competed by the high concentration of nitrate. This concurs with previous observations for polyamine resins [14]. At alkaline pHs, Cu leaching was most severe at pH 12. At pH 13 however, although iodide uptake remains low, Cu leaching is decreased substantially. An XRD spectrum of the spent resin sample at pH 13, revealed the precipitation of both CuO and Cu_2O within the resin macropores. Yet at pH 12, the diffractogram was completely amorphous, as were samples at all other pHs (Fig. S1). At pH 12, the coordinated Cu^{2+} is hydrolysed by base, but is kept from precipitating by the high solution iodide concentration and instead undergoes reduction (Eqs. (1)–(3))

$$Cu^{2+} + 2I^- \rightleftarrows CuI_2 \quad (1)$$

$$2Cu_2 \rightleftarrows 2CuI + I_2 \quad (2)$$

$$CuI + I^- \rightleftarrows [CuI_2]^- \quad (3)$$

The small quantity of molecular iodine formed would immediately associate with the organic resin, hence the lack of iodine coloration observed in the solution and this explains why there is still some measured uptake of iodide. At pH 13, the $[OH^-]$ competes with the iodide in these equilibria and precipitation of copper oxides does occur.

The ideal pH for iodide adsorption was 2–3. This is likely influenced by the pK_3 of a small number of uncoordinated aliphatic ammonium groups [30]. These would allow chloride/iodide anion-exchange, without excessive competition from nitrate, leading to a slight additional uptake. For future experiments, it was observed that the resin mass naturally buffered the contact solutions to a pH of ~2.5. Given these favourable uptake conditions, no further attempt was made to control the pH of the system.

3.3. Determination of maximal uptake of iodine species by isotherm

Isotherms were produced to assess the equilibrium static capacity of M4195-Cu. Both iodide only and mixed iodide/iodine systems were studied, results being shown in Fig. 3. In the latter case, the molar ratio of iodide to iodine was 1:6. This was set, not to attempt to mimic industrial conditions, but to clearly elucidate the different uptake characteristics of an iodine-dominated aqueous phase. Data were fitted with four common two-parameter isotherm models, which are introduced and described in the Supporting Information, p2-3. Such models have previously been applied to describe adsorption by metallated extractants [19,24,33]. Data fitting used non-linear least squares analysis, with the Microsoft SOLVER add-in [34]. The errors associated with the isotherm adsorption parameters (Table 2) were determined using the associated SolvStat macro [34].

For both systems, the uptake of iodide alone was well described by the classical Langmuir model. This was unexpected, since it is clear from the theoretical uptake mechanism (Fig. 1) that two heterogeneous

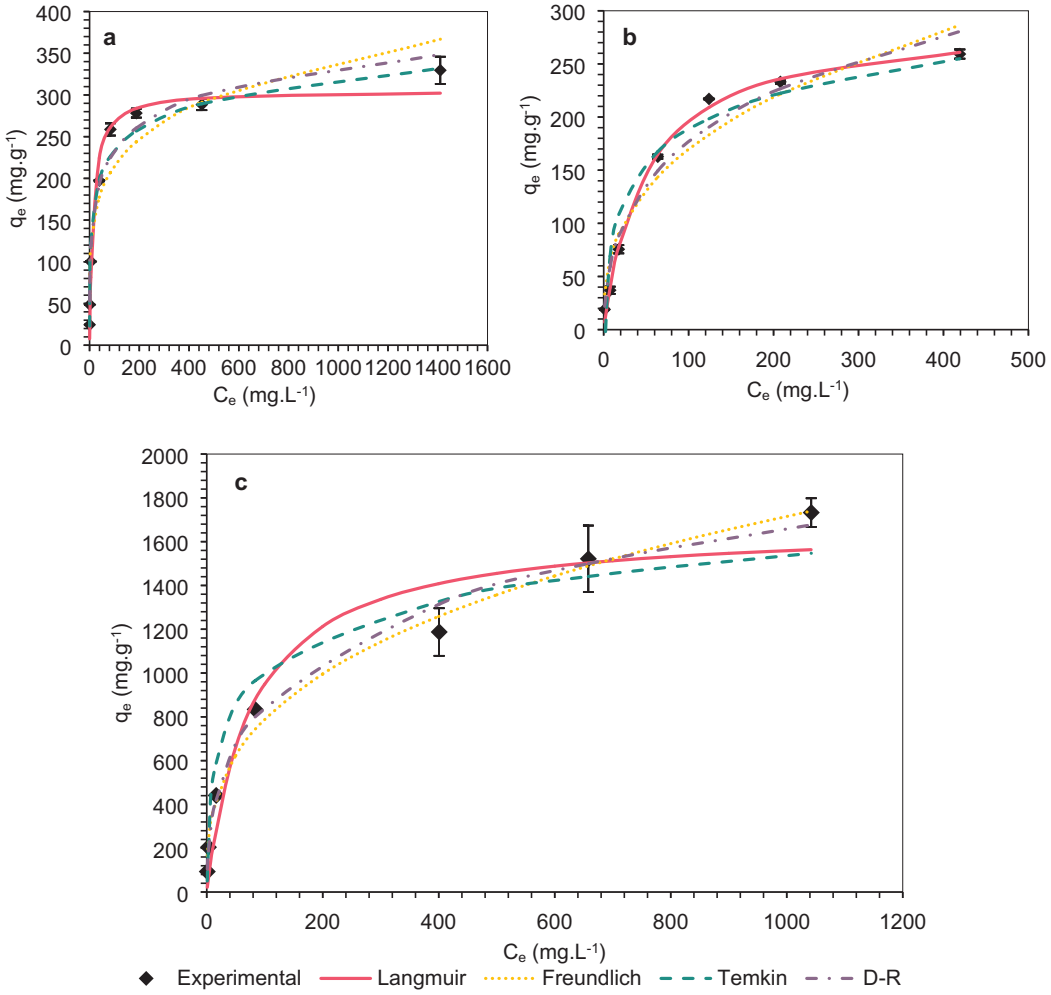

Fig. 3. Uptake isotherms of iodine species on to M4195-Cu with fitting to common thermodynamic models. **(a)** Iodide only system. **(b)** Iodide uptake only from mixed iodide/iodine system. **(c)** Total iodine uptake from mixed iodide/iodine system. Initial [I^-] = 50–2000 mg.L^{-1}. Initial [I_2] = 300–6000 mg.L^{-1}. Error bars represent approximate 95% confidence intervals derived from 2 × experimental reps.

Table 2
Extracted parameters from isotherm models for uptake of iodine species by M4195-Cu.

Model and parameter	NaI solution (I^- only)	NaI/I_2 solution (I^- only)	NaI/I_2 solution (total I)
Langmuir			
q_{max} (mg.g^{-1})	305 ± 14	291 ± 8	1680 ± 690
K_L (L.mg^{-1})	7.09 ± 2.0 × 10^{-2}	2.05 ± 0.21 × 10^{-2}	1.30 ± 0.11 × 10^{-2}
R^2	0.974	0.996	0.958
Freundlich			
K_F	84.3 ± 18	31.2 ± 10	166 ± 3
n	4.93 ± 0.86	2.72 ± 0.45	24.2 ± 0.2
R^2	0.891	0.931	0.991
Temkin			
A_T (L.mg^{-1})	5.09 ± 2.9	0.579 ± 0.25	0.787 ± 0.36
B	0.295 ± 0.020	0.366 ± 0.044	1.82 ± 0.18
b_T (kJ.mol^{-1})	8.41 ± 0.24	11.2 ± 0.7	1.34 ± 0.13
R^2	0.975	0.933	0.952
Dubinin-Radushkevich (D-R)			
q_{max} (mg.g^{-1})	456 ± 37	638 ± 96	2940 ± 180
B_D (mol^2.J^2)	2.15 ± 0.29 × 10^{-9}	4.10 ± 0.54 × 10^{-9}	3.94 ± 0.30 × 10^{-9}
E_{des} (kJ.mol^{-1})	15.3 ± 1.0	11.0 ± 0.7	11.3 ± 0.42
R^2	0.948	0.962	0.991
Experimentally-determined q_{max} (mg.g^{-1})	330 ± 16	259 ± 4	1730 ± 70

ligand-exchanges must be involved in forming the BPA-CuI_2 complex. We must assume that both ligand-exchanges are so rapid that any heterogeneity is too subtle to be observed from thermodynamic data and therefore the overall effect is a pseudo-degenerate interaction. Indeed, Sutton reported that the analogous aqueous complex formed instantaneously [25]. The Langmuir theoretical saturation uptake capacity (q_{max}) was nonetheless considered more valid that the equivalent Dubinin-Radushkevich (D-R) parameter. For the iodide-only experiments, the q_{max} value, converted to $mmol.g^{-1}$ is 2.45 ± 0.07, which notably, is almost exactly twice the Cu-loading value of M4195 (Table 1). This gave a theoretical loading efficiency of 97.7%, assuming one Cu centre coordinates two iodide ligands (Fig. 1). The observed adherence to the Langmuir model implies that iodide uptake by M4195-Cu, within these idealised systems, proceeds via monolayer formation and interaction with degenerate binding sites [35]. However, the Langmuir equilibrium constant (K_L) was significantly higher for the iodide only system, implying a stronger interaction. This is supported by the differing desorption energy (E_{des}), as calculated by the D-R model. It is known that an E_{des} value of $< 8\ kJ.mol^{-1}$ is representative of physisorption and 8–16 $kJ.mol^{-1}$ representative of an ion-exchange loading interaction [35–37]. For the iodide only system, the value of 15.3 ± 1.0 is towards the top end of this range and closer to the region $> 16\ kJ.mol^{-1}$, implying chemisorption [19], which is sensible for a ligand-exchange reaction. The Langmuir K_L value (iodide-only system) is similar to the range reported by Nie *et al.*, for uptake of fluoride, via ligand-exchange by an Al-loaded adsorbent [38] It was unknown at this point whether the change in iodide affinity was due to an altered uptake mechanism in the iodide/iodine system, or whether the presence of iodine was simply modifying the hydrophobicity of the aqueous phase and affecting iodide partitioning. The Temkin model also provided a good description of the uptake of iodide. Thus, it is ambiguous from these data, whether the uptake sites were truly degenerate, or whether the heat of adsorption decreased linearly as a function of surface coverage [39]. It can however be seen, from lack of agreement with the Freundlich model, that iodide extraction was not a multilayer adsorption process.

For total iodine uptake however, the reverse was true, with the Langmuir model providing inadequate description, and the D-R q_{max} was considered the more valid parameter. This implies that the uptake was more heterogeneous than for iodide considered in isolation. The dissolution of iodine in iodide solutions causes an equilibrium to form with the triiodide anion (Eq. (4)):

$$I^- + I_2 \rightleftarrows I_3^- \quad (4)$$

It is known that both triiodide and iodine readily act as σ-acceptors in the formation of stable charge-transfer (CT) complexes with both amines [40,41] and small aromatic ring structures [42]. Clearly, the massive uptake of total iodine cannot be accounted for by ligand-exchanges only with metallated functional groups, so the apparent heterogeneity of uptake is predictable. The Freundlich n parameter (a measure of the heterogeneity of an adsorption system) is notably an order of magnitude higher for total iodine uptake than for iodide uptake alone.

A comparison of performance between M4195-Cu and relevant extractants from the literature is seen in Table S2. M4195-Cu is highly competitive in terms of maximal iodide adsorption, with only the polyamine resins from our previous work offering higher capacity [14]. We also note that the total iodine capacity is of the same order of magnitude as that of porous aromatic frameworks (PAFs) at 2,760 $mg.g^{-1}$, conjugated microporous polymers (CMPs) at 3,450 $mg.g^{-1}$ and metal organic frameworks (MOFs) at 1,010 $mg.g^{-1}$), which were synthesised specifically for gaseous iodine capture [10,11,43]. The uptake of aqueous mixed iodine species by IX resins has been rarely studied. Hatch *et al.* reported that a commercial strong base anion (SBA) resin could adsorb triiodide equivalent to 97% of its quoted exchange capacity [44]. They also found that adsorption was almost irreversible when the ammonium was directly bound to the resin matrix via a benzyl group, as is the case for the aliphatic amines of M4195 (although in our work, of course, the great majority of these will be coordinated to Cu). Aliphatic anion-exchange resins and unfunctionalized resins did appear to bind iodine, but with much weaker interactions [44]. Lambert *et al.* found that triiodide-loaded SBA resins could be converted to polyiodide forms (I_5^- and I_7^-) by treatment with excess iodine, which was considered a possible explanation for the enhanced uptake observed in this case [45]. Sanemasa *et al.* studied the uptake of aqueous iodine via SBA and strong acid cation (SAC) resins [46]. Extrapolation of their results, which were attained at low [I_2], suggest that the total iodine capacity of M4195-Cu is an order of magnitude higher than a SAC resin, but 2 orders of magnitude below a SBA resin. From this, we postulated that the small fraction of quaternised aliphatic amines, which are non-chelating [30] were probably the main binding sites for iodine and triiodide.

3.4. Investigations into competition effects of nitrate and molybdate

The effect of cocontaminants nitrate and molybdate on the uptake of iodide (in each case, up to a ten-fold molar excess) under static, equilibrium conditions was assessed. For each experiment, the distribution coefficient (K_d) for all three anions, as a measure of partitioning between the aqueous phase and resin was calculated (Eq. S6, Table S3). The separation factors (S.F.) were also determined, giving a measure of the affinity of M4195-Cu for each anion, at each molar ratio (Eq. S7). Fig. 4 summarises the uptake trends for each species. As seen, the affinity for iodide was resistant to the challenging conditions, with the resin retaining > 50% of its usual capacity even with 10 added molar equivalents of each cocontaminant. Nitrate uptake was uniformly low, with large S.F.s calculated for iodide verses nitrate ($Cu(NO_3)_2$ K_{sp} = 2,440), whereas molybdate was a more significant suppressor ($CuMoO_4$ $K_{sp} = 2.8 \times 10^{-7}$). The full dataset is shown in Table S4 and Fig. S2. However, the linear decrease in performance with increasing mass of cocontaminant we observed with non-metallated polyamine resins [14] did not occur; rather, the suppression reached a plateau at ~4 M equivalents of nitrate and molybdate (Fig. 4 inset). The resin thus retained some selectivity for iodide even at high levels of cocontaminants. This suggested the reduction of a small proportion of the Cu centres was occurring: a large number of stable Cu(I) halide complexes are known [47], while Cu(I) molybdate complexes are rare and tend to involve the higher molybdates rather than $MoO4^{2-}$ [48]. These experiments also revealed that the molar amount of chloride released into solution always exceeded the equivalents of anions adsorbed by the resin, which is likely residual chloride present in the original M4195 material. Chloride does not appear to act as an inner-sphere ligand on the bound Cu centres and at least partially dissociates in the aqueous phase. This is concurrent with early synthetic work on BPA-Cu halide salts [25]. Similarly, it was proven by Spencer *et al.* that Cu centres, coordinated to a solid-phase BPA group via treatment with $CuSO_4$, possessed aqua ligands, with sulfate acting as an uncoordinated outer-sphere anion [29].

3.5. Dynamic experiments

Dynamic column studies simulate the use of resins and other adsorbents in industry. The performance of M4195-Cu was tested with a simple iodide-only inlet solution, to gauge the maximum dynamic uptake capacity, but also with added nitrate and molybdate at 10 M equivalent ratios, to examine the dynamic response to cocontaminants. We also subjected a column of polyamine Purolite® MTS9850 resin, from previous work [14], to this mixed-species inlet solution, for comparison. Breakthrough curves can be fitted with various models, which allow calculation of useful hydrodynamic parameters. The Modified Dose-Response and Adams-Bohart models were applied in this instance, which are introduced and described in the Supporting

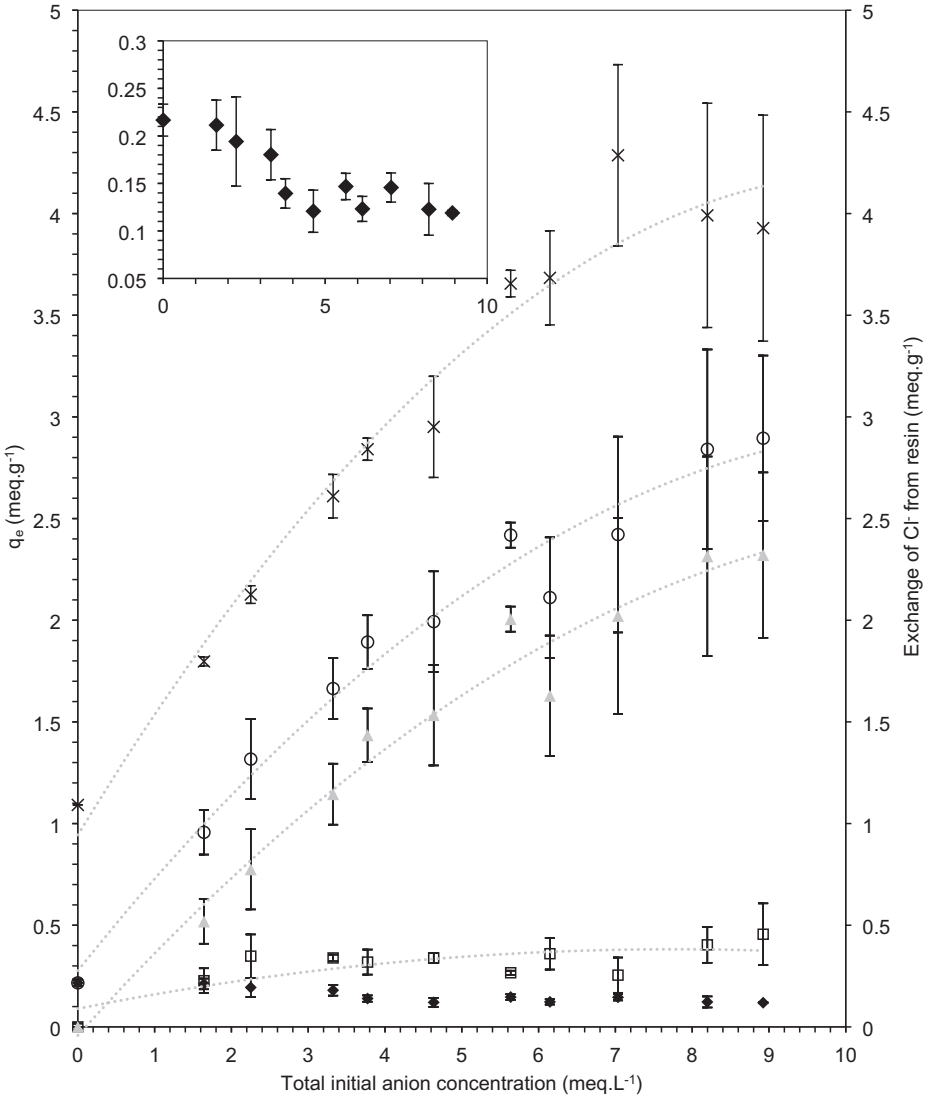

Fig. 4. Uptake of iodide (◆), nitrate (□), molybdate (▲) and total anions (○), with accompanying release of chloride (×) in mixed anions systems. 2nd order polynomial fits added to guide the eye. Inset shows enlargement of iodide uptake data. Initial [I^-] = 50 mg.L^{-1}. Cocontaminant molar ratio = 0–10. Error bars represent approximate 95% confidence intervals derived from 2 × experimental reps.

Information, p6. Data-fitting was again achieved using SOLVER, with error calculation via SolvStat [34]. Results for both systems are presented in Fig. 5 and the extracted parameters shown in Table 3. In the case of the column with cocontaminants, the breakthrough could not be well-described by a single curve, but instead reached an initial plateau, with [I^-] at ~70% of the inlet concentration, before full breakthrough was reached (For reference, the raw dataset for column experiments can be seen in Figs. S4 and S5). This infers that there are two discrete

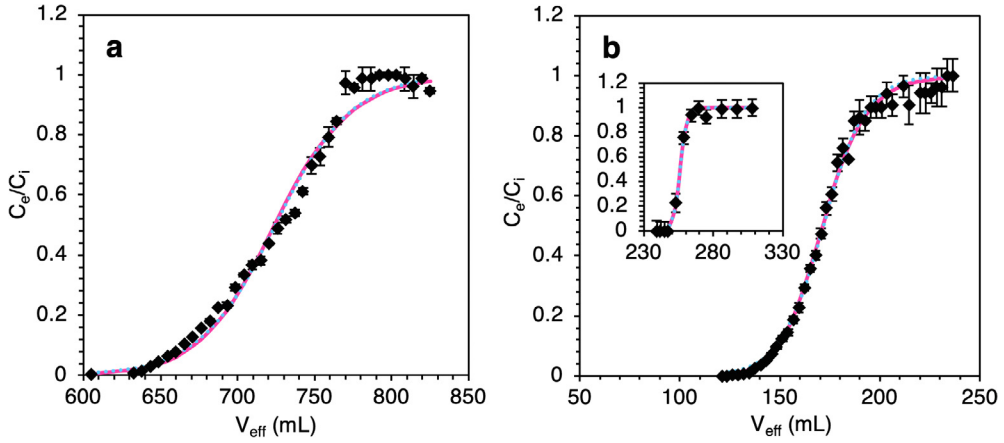

Fig. 5. (a) Breakthrough curve for M4195-Cu with an iodide only solution. **(b)** Breakthrough curves for M4195-Cu with iodide, 10 meq nitrate and 10 meq molybdate solution (main graph shows 1st breakthrough, inset shows 2nd breakthrough). Data fitted to the Dose-Response (pink line) and Adams-Bohart (dotted blue line) dynamic models. Inlet [I^-] = 2.00 g.L^{-1}. Error bars represent the approximate 95% confidence intervals, derived from 3 × electrode measurements. (For interpretation of the references to colour in this figure legend, the reader is referred to the web version of this article.)

Table 3
Extracted parameters from modelling of breakthrough data, with experimental conditions as per Fig. 5. For S985 column, values are for the initial stages of breakthrough only.

Model/parameter	Iodide only	Iodide and cocontaminants (1st breakthrough region)	Iodide and cocontaminants (2nd breakthrough region)	Iodide and cocontaminants (MTS9850)
Modified Dose-Response				
a	29.5 ± 1.4	15.9 ± 0.5	109 ± 9	15.1 ± 0.6
b	724 ± 1	171 ± 4	256 ± 3	63.8 ± 0.2
q_0 (mg.g^{-1})	356 ± 6	114 ± 2	46.5 ± 0.4	50.4 ± 0.1
R^2	0.986	0.996	0.997	0.996
Adams-Bohart (AB)				
k_{Th} (mL.min^{-1}.mg^{-1})	3.74 ± 0.16 (× 10^{-6})	6.43 ± 0.21 (× 10^{-6})	1.07 ± 0.09 (× 10^{-4})	1.39 ± 0.05 (× 10^{-5})
q_0 (mg.g^{-1})	401 ± 7	128 ± 3	52.3 ± 0.5	56.8 ± 0.1
R^2	0.988	0.995	0.997	0.997

binding sites on the resin surface, one of which has a greater resistance to competitive molybdate uptake. These could be correlated to the two different loaded Cu environments (coordinated to either one or two BPA groups) [29]. The effect of the heterogeneous binding sites cannot be seen in the iodide-only column experiment, because iodide adsorption is not hindered by the competitive coadsorption and the higher ionic strength, which has been shown to retard dynamic adsorption kinetics [49]. This would also explain why the iodide-only isotherm (Fig. 3a) also does not show the predicted heterogeneous binding. Both breakthrough regions could successfully be modelled individually and for both systems, the breakthrough curves for M4195-Cu were adequately described by both models. The Dose-Response model is empirical in nature and does not provide insights into the nature of the adsorption. The close agreement with the Adams-Bohart model implies that the uptake process is highly favourable and suggests 2nd-order kinetics, rate-limited by interfacial mass-transfer, rather than chemical reaction [50–52]. This is predictable, as the inner-sphere ligand-exchanges for aqueous Cu^{2+} are extremely rapid, occurring in ~200 ps [53]. The AB rate constant (k_{AB}) was of the same order of magnitude as equivalent experiments conducted with a La-loaded resin, which similarly removed fluoride via ligand-exchange reactions [51].

The MTS9850 breakthrough curve (Fig. S3) shows the strong suppression of iodide uptake by the cocontaminants, as the effluent [I^-] exceeded that of the inlet as part of the breakthrough process, as iodide that is initially bound by ion-exchange is ultimately displaced by the divalent molybdate ions as the system approaches equilibrium. Because of this, the models were unable to adequately describe the breakthrough and the calculated q_0 values for MTS9850 are overestimates, as they do not account for the iodide bleeding from the column. Even so, it can be seen that, under more realistic conditions, the working capacity of M4195-Cu (though reduced by ~55% compared to the iodide only system) far exceeds that of the polyamine resin. Interestingly, the q_0 values obtained for the iodide only column were in excess of the equilibrium q_{max}, determined by Langmuir isotherm. The implications for the uptake mechanism are discussed in 3.8.

3.6. Solid-state resin characterisation for investigation of uptake mechanisms

A number of spectroscopic techniques characterised the resin, at different process stages, providing insights into the uptake. FTIR spectra, along with assignments for the bands observed, are shown in Figs. S6–7 and Table S5-6. It can be seen that the bond vibrations associated with the pyridyl and aliphatic amine groups change, due to lone-pair donation, as the Cu-BPA complex is formed. The M4195-Cu spectrum was largely unchanged by the binding of iodide. However, interesting variations were observed in the N–H st. region (~3400 cm^{-1}) and N–H bend region (~1680 cm^{-1}). Upon Cu coordination, the former peak does not decrease in intensity, even though there is necessarily a reduction in N–H bonds. So it can be assumed (as predicted) that the Cu centres coordinate two aqua ligands, rather than chlorides, and there is a contribution of the O–H st. to this region [29]. Upon iodide binding, there is a marked reduction of peak intensity, from which we infer that iodide ligands do indeed coordinate directly to the Cu centres, displacing aqua ligands. This is predictable from the literature [25,54] and confirms the high strength of binding interaction seen from calculated isotherm parameters. Upon contact with the iodide/iodine mixture, the N–H st. and N–H bend regions remarkably almost completely disappear and a new unidentified peak appears at 1739 cm^{-1}. We assign this behaviour to formation of the triiodide CT complex on the resin surface. Triiodide is strongly attracted to amines, due to a favourable σ-donor (amine)/σ-acceptor (I_3^-) interaction [40,55]. We observed this behaviour in previous work with polyamine resins [14]. Refat *et al.* reported comparable spectral changes in the formation of a morpholine-I_3^- CT complex [40]. We conducted an experiment (Supporting Information, p10), to investigate the number of protons liberated from the resin surface, during contact with iodide and iodide/iodine solutions. From this, it was clear that some uncoordinated ammoniums are deprotonated in the formation of the CT complexes, which explains the FTIR spectra produced.

RAMAN spectroscopy confirmed the presence of triiodide on the spent resin surface (Fig. S9). The symmetrical stretch of the triiodide anion, after resin contact with the iodide/iodine solution, was observed at ~111 cm^{-1}, with the asymmetrical stretch at ~155 cm^{-1} being a weakly visible shoulder peak. This is higher than observed in previous work (150.7 cm^{-1}) [14], but is somewhat variable in wavenumber [56]. Unexpectedly, the sample contacted with iodide only produced an equivalent spectrum, which suggested an in-situ REDOX process, unique to M4195-Cu, was occurring at the resin/solution interface We also attained RAMAN spectra for MTS9850, featured in previous work and, while the iodide/iodine-treated sample exhibited characteristic triiodide peaks, the iodide-treated sample spectrum was completely featureless (Fig. S11). There was no evidence in any spectra of higher iodides or molecular iodine [57].

Solid state NMR spectra are shown in Figs. S12–14. The ^{13}C spectra show the expected aliphatic (δ 30–65 ppm) region, representing the alkyl polymer chains and crosslinkers, and aromatic (δ 120–160 ppm) region, representing the phenyl and pyridyl rings. For M4195 samples, a minor peak is present at δ 60 ppm, which is assigned to the –CH_2- carbons between the functional group tertiary amine and pyridyl/phenyl rings. In M4195-Cu samples, this peak shifts to lower δ and is indistinguishable from the other aliphatic carbons; probably a result of increased shielding from the nitrogen atom, as its lone pair is now involved in a coordinate bond. The most de-shielded carbons (next to the pyridyl nitrogen) see a similar small shift, from δ ~149 to ~145 ppm. The binding of iodine produced no discernible change in the ^{13}C spectra. Unfortunately, only non-Cu-loaded samples had sufficient signal to noise ratios to produce interpretable ^{15}N spectra. Nonetheless, three distinct environments were observed. The broad signal at δ ~50 ppm was assigned to the protonated and permanently quaternised

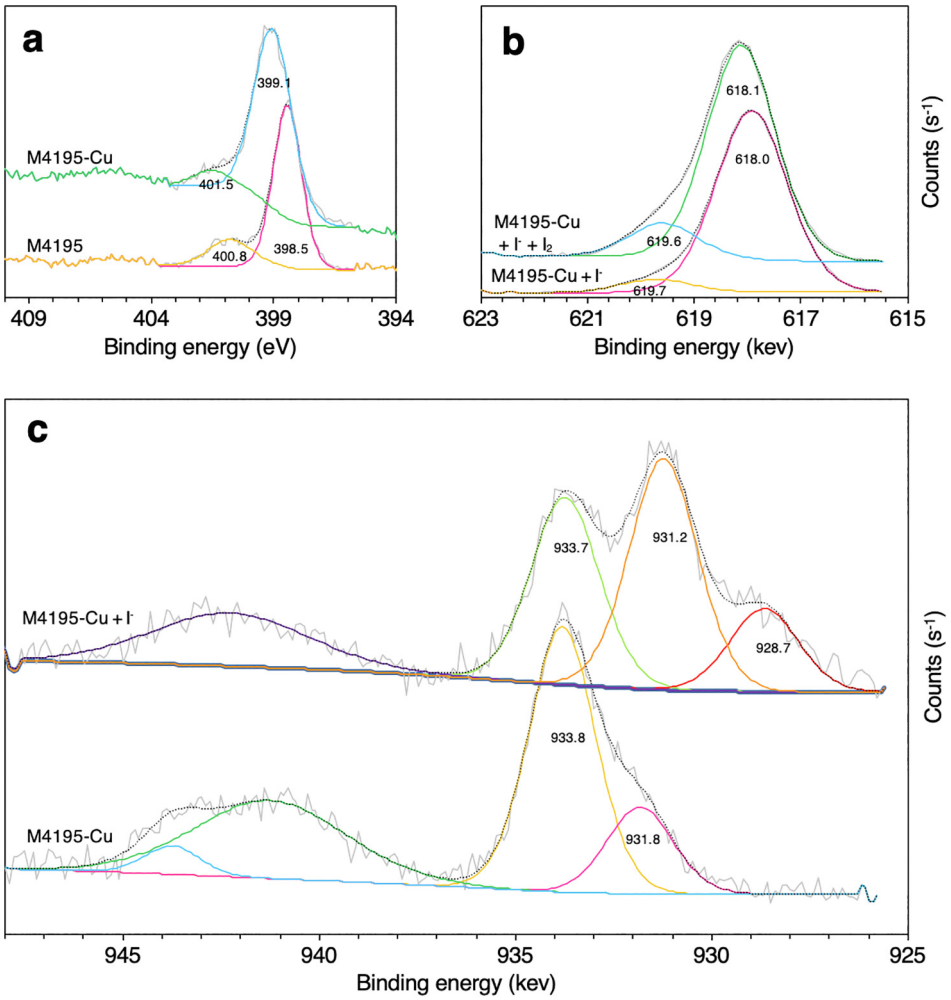

Fig. 6. Selected high resolution XPS spectra of M4195 resin, at various processing stages: **(a)** N 1 s, **(b)** I 3d, **(c)** Cu 2p 5/2. For samples contacted with solutions of iodine species, initial $[I^-] = 1{,}000\ mg.L^{-1}$. Initial $[I_2] = 6{,}000\ mg.L^{-1}$.

ammoniums, whilst those at δ ~208 and 315 ppm were assigned to neutral and protonated pyridyl nitrogens respectively. This appears to confirm that the degree of protonation of the functional group predicted by Ogden *et al.* (an equilibrium between the mono- and di-protonated ligand forms at pH ~2) for M4195 was correct [22]. We also note that, for the M4195 sample contacted with I^-/I_2 solution, the aliphatic ammonium peak is shifted to lower δ, whereas the pyridyl amine/ammonium peaks are not. This could indicate that CT complexation with triiodide occurs, as previously proposed, mainly at aliphatic sites [41], (although we should note, it is not proven that the uncoordinated ammonium environment responds similarly in an M4195-Cu sample).

XPS survey scans provided information on the atomic composition of samples (Table S7). It can be seen that the atomic ratio of Cu:Cl for M4195-Cu is almost exactly 1:2, whereas for the iodide-loaded samples, the ratio is ~1:1.3, which may support the assumption that some Cu reduction takes place as part of the exchange process. Interestingly, no Cl was detected in M4195 samples, indicating the chloride present in M4195 is displaced from the surface by sulfate, during a later manufacturing step [26], but still present in pore interiors, diffusing out when the resin is properly hydrated.

Selected high resolution scans of N 1 s, Cu 2p and I 3d are seen in Fig. 6. It can be seen that XPS is not as discriminatory between nitrogen environments as NMR, as all of the electron-rich pyridyl nitrogens (protonated and neutral) in the M4195 sample are represented by a single peak at 398.5 eV [58], with the quaternary ammoniums appearing as a shoulder, at 400.8 eV. These are lower than expected binding energies [58], but we have observed similar traits for amines in polymeric resins [19]. However, upon Cu-chelation, all environments are shifted to a higher binding energy by 0.6–0.7 eV, again indicating lone pair involvement in metal bonding.

The Cu 2p spectrum (Fig. 6c), for a sample prior to iodine contact, shows two Cu(II) environments (predicted by dynamic uptake studies), the minor at low binding energy. This is believed to represent doubly-chelated Cu centres, anchored between two BPA groups [29], with more N-donors providing extra electron density, as was proposed from the Cu-loading data. The spectrum changed remarkably upon contact with iodide, as the main Cu(II) environment remains, but a new peak and shoulder appear at 931.2 and 928.7 eV. This, along with a reduction in the area of the satellite region, suggests strongly that Cu(I) is indeed formed as part of the iodide uptake process [59]. We also note that, for the peaks thought to represent the doubly-chelated environment, for the pre- and post-iodine-contact samples, the % of total Cu is almost equivalent (Table S9). It appears that all of the doubly-chelated and ~60% of the singly-chelated Cu centres are reduced by treatment with iodide. From this data, we propose that the doubly-chelated sites possess the greater affinity for iodide-binding and are more resistant to competitive molybdate adsorption. This would explain why, in the dynamic loading experiment (Fig. 5b), full column breakthrough is achieved in two discrete stages, with the number of higher affinity sites seemingly being proportionately lower. It should be noted however that XPS spectra may reflect the degree of REDOX on the resin surface only, rather than in the bulk of the material. It has been reported that mixed

Cu(I)/Cu(II) products can result from in-situ Cu reductions, by iodide, to form coordination polymers [60]. Therefore, this behaviour is plausible in a disordered polymer matrix. The factors governing Cu reduction are numerous, including choice of solvent, anion and reducing agent. However, it has been seen that a more hydrophobic coordination environment promotes irreversible reduction [61]. The exact coordination mode of doubly-chelated Cu is not known, but there is likely more, or even total exclusion of aqua ligands [29], making reduction more favourable. The apparent increase in [Cu] upon iodide uptake is due to the extent of reduction, meaning many less ligands and counter anions are present on the sample surface.

The I 3d spectra showed the dominant surface species to be iodide. This is not likely to accurately reflect the uptake (especially given the RAMAN spectra), because of loss of more volatile iodine species in the XPS vacuum. Nonetheless, there was a second, more electron-poor environment detected. From the literature, this could represent either iodine [62] or triiodide [63]. These more hydrophobic species are known to migrate towards the centre of IX beads during uptake [44], potentially avoiding being completely volatilised. Another possibility is that this environment simply represents an iodide ligand shared between two Cu centres [60,64] and all iodine, apart from Cu inner-sphere-coordinated iodide ligands, is volatilised.

3.7. Desorption studies

To clarify the iodine speciation on the resin surface, we attempted back-extraction by contacting the spent resin beads with methanol (Supporting Information, p15-17). The desorbed iodine in solution was characterized by UV–Vis spectroscopy. (Fig. S15). The spectra showed the expected peak at 221 nm, characteristic of iodide, peaks at 290 and 361 nm, corresponding to triiodide (spin orbital split bands) and ~445 nm, corresponding to molecular iodine [65,66]. For M4195 samples, peaks were observed at ~260 and 345 nm, which were attributed to some slight leaching of a contaminating resin functionalisation reactant, most likely an aromatic amine, and not related to iodine species. It can be seen that no iodine species at all are extracted from the M4195-Cu + I^- sample, but a large quantity of triiodide is leached from the M4195-Cu + I^- + I_2 sample. This suggests that, although triiodide is formed on the resin surface in both instances, the mechanism of binding is different. Samples of M4195 (not Cu-loaded) + I^- and MTS9850 + I^- both released iodide during back-extraction, confirming the comparative very high-strength binding environment of the Cu centres. Interestingly, although M4195 + I^- + I_2 and MTS9850 + I^- + I_2 both leached triiodide, the loss was two orders of magnitude less than for M4195-Cu. This appears to confirm the postulation of Hatch *et al.* [44] that strong binding of triiodide to a resin requires quaternary ammonium groups in proximity to phenyl rings [14], with metal-coordinated amines evidently not producing the same effect. Crucially, there was no molecular iodine present from the leaching of any of the resin samples (Figs. S15 and 16), which strongly suggests that polyiodides were not formed in significant quantities by the uptake process [65].

3.8. Proposed binding mechanisms

With respect to the M4195-Cu/iodide system, the evidence is clear that in-situ REDOX chemistry is occurring, forming Cu(I) and triiodide (Fig. 7). We must therefore conclude that the resulting 2:1 molar ratio of I:Cu on the spent resin, deduced from isotherm experiments (Tables 1 and 2), is coincidental and the uptake mechanisms are more diverse than shown in Fig. 1. The triiodide is fully bound to the resin and does not remain in solution to any significant degree. This was obvious from lack of coloration, but we confirmed it with several analyses of post-contact solutions, for which we quantified both iodide and total iodine with ISE and ICP-MS (not presented). The figures were always in agreement within 5%. The triiodide binding is of sufficient strength to resist methanol back-extraction, but not volatilisation under vacuum. This explains why the resin-bound I:Cu ratio, calculated by isotherm, is higher than that seen in XPS experiments (Table 2 and S7). Because of the substantial percentage of Cu reduction, it is impossible that the triiodide formed is taken up entirely by the small number of non-coordinating quaternary ammoniums remaining on the resin. Therefore, it is suggested that the triiodide principally interacts with the Cu centres themselves. It is very unusual, (though not impossible), for higher iodides to act as inner-sphere Cu ligands via end-on coordination and they tend to appear as counter-anions to Cu complexes [60,64]. X-ray absorption fine structure (EXAFS) spectroscopy may elucidate the triiodide behaviour in this regard, but is beyond the scope of this study.

In dynamic experiments (considering the iodide only system), the experimental flow rate was obviously sufficiently low for the ligand-exchange reaction to equilibrate in the active region of the column, but sufficiently high to avoid excessive REDOX chemistry occurring. This explains why the M4195-Cu dynamic uptake capacity unusually exceeded the equilibrium uptake capacity.

In the case of the M4195-Cu/iodide/iodine system, the uptake quantity and weak nature of the adsorption (Fig. 3c) cannot be explained by interaction only with the relatively small concentrations of ammoniums or Cu present (as it has been proven that formation of higher iodides on individual binding sites does not occur). Instead, we must conclude that the iodine merely associates with the plentiful aromatic rings of the polymer matrix, forming triiodide CT complexes and leading to the very large uptakes observed. The spectroscopic evidence for this is more limited. However, we did acquire additional KBr disc FTIR spectra for M4194-Cu samples pre- and post-contact with the iodide/iodine solution, for better resolution of the C–H st. region (Fig. S8). From these, it can be seen that these peaks reduce in intensity, comparative to the rest of the spectrum, which has been suggested to indicate the predicted CT interaction [14,67]. In XPS C 1 s spectra, we also observed peak-broadening of the aromatic environment for the post-contact sample (data not shown) with FWHM increasing from 1.95 to 2.05 over all other samples tested.

3.9. Investigations into conversion to final wasteform

With most adsorbents, the ability to be recycled and retain operating capacity over numerous regenerations is important [21,24,51,67]. Yet, within our remit, the spent IX resins would be radioactive. Therefore, consideration of wasteform and disposal is more pragmatic. One option for resin waste is cementation. However, the swelling and shrinking properties of IX beads in the matrix cause loss of compressive strength and lead to leaching [68]. Incineration or pyrolysis, converting the resin to inorganic ash prior to cementation, has been used industrially [69], but relies on the radionuclides remaining with the ash, rather than volatilising. Other techniques, such as bituminization also require stability at elevated temperature. We therefore studied the thermogravimetric behaviour of the resins (Fig. 8), in conjunction with XRD analysis of the decomposition products, to check for iodine volatilisation.

The thermal decomposition of IX resins, under oxidising conditions, proceeds in two main stages; the first, at ~270 °C decomposing the functional groups and the second, at ~480 °C combusting the hydrocarbon skeleton [70]. The M4195 thermogram follows this behaviour closely. When dosed with iodide and iodine, the onset of the first decomposition comes at reduced temperature, possibly because of the effect of CT complex formation on the BPA functionality. Iodine appears to be lost in two stages at 360 and 395 °C (confirmed by observation of purple vapour), which shows that the triiodide ions are strongly held by the protonated amine matrix (T_{sub} for I_2 = 183 °C at atmospheric pressure). The M4195-Cu sample showed similar decomposition to M4195, but with much greater mass retention after the loss of the polymer matrix. When loaded with iodide, M4195-Cu seemed to lose a small quantity of bound iodine over the 360–395 °C range, which may

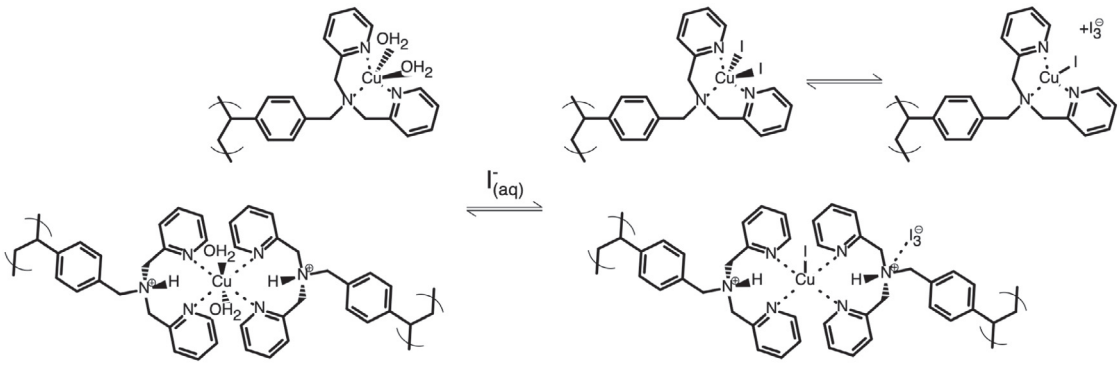

Fig. 7. Proposed loading mechanisms of iodide on to M4195-Cu.

be attributed to non Cu-associated triiodide; but the majority is retained up to 850 °C, further evidencing the strength of binding interaction. M4195-Cu, after iodide *and* iodine loading, exhibited a very different thermogram, with loss of iodine occurring at 180 and 305 °C (suggesting the weakest interactions of all the samples). Nonetheless, from the remaining mass %, there did still seem to be appreciable iodide (surely as Cu ligands) retained up to 850 °C. The iodine volatilisation behaviour is similar to that reported for a Cu(I) coordination polymer, with non-coordinated triiodide [60] The thermal stability of the adsorbed iodine species thus seems to mirror the chemical stability.

XRD spectra were collected for iodide- and iodide/iodine-treated samples combusted at 350 and 600 ± 25 °C (below and above the decomposition temperature of the polymeric resin). While M4195 and MTS9850 samples were all completely amorphous, the M4195-Cu samples, after 350 °C heating, revealed clear CuI and CuO peaks (Fig. S16). M4195-Cu samples, after treatment with cocontaminants, also showed $CuMoO_4$ peaks [27]. After 600 °C heating, no CuI was present in the ash, but analysis of the silica crucibles (Fig. S17h) revealed that the CuI (T_m = 606 °C) had fused with the crucible and the iodine had not volatised. Overall, the thermal analysis indicated that, despite the high capacity of M4195-Cu for multiple iodine species, their uptake (rather than iodide alone) may ultimately be contrary to the goal of preventing volatility and entrapment within a final wasteform. Future process optimisation will focus on converting the majority of iodine species in the wastestream to iodide.

4. Conclusions

Aqueous iodide adsorbs on to solid-phase Cu-loaded bispicolylamine groups via inner-sphere ligand exchange and with high binding strength. We have demonstrated this via Cu-loaded M4195 chelating resin, for potential applications within the nuclear industry. The maximal loading of this adsorbent (305 $mg.g^{-1}$ equilibrium capacity, 356 $mg.g^{-1}$ dynamic capacity) exceeds others reported in the literature. It has a broad working pH range and displays good resistance to competitive coadsorption by nitrate and molybdate; even with these anions present at 10 molar equivalent concentrations. The uptake process causes an in-situ REDOX reaction, leading to the dominant species on the spent resin being Cu(I). Although this reduced the ultimate iodide capacity of the resin, it was likely beneficial to its

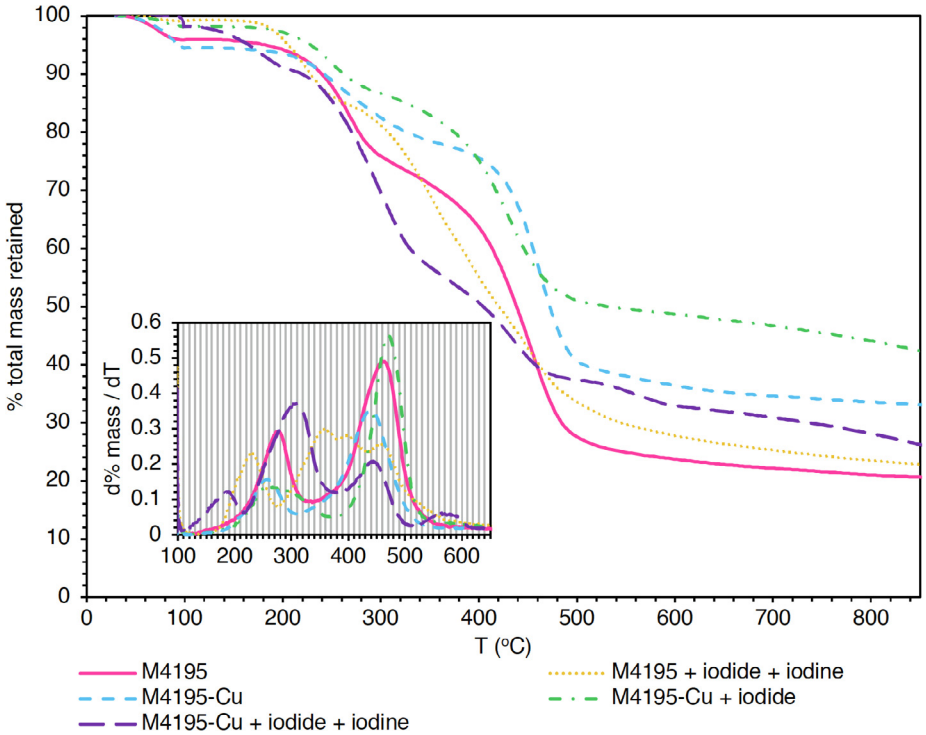

Fig. 8. Thermograms of M4195 resin samples at various processing stages, in oxidising conditions. Inset shows first derivative. For samples contacted with solutions of iodine species, initial $[I^-]$ = 1,000 $mg.L^{-1}$. Initial $[I_2]$ = 1,000 $mg.L^{-1}$.

resistance to cocontaminant uptake. The triiodide generated was immediately coadsorbed, also with unusual binding strength. In mixed iodide/iodine systems, the uptake mechanism was different and likely involved triiodide charge-transfer complex formation with the resin phenyl groups, causing very high uptake capacity (2940 $mg.g^{-1}$). Although chemically interesting, the relative weakness of binding would likely cause problems during thermal treatment of waste, due to iodine volatility; whereas the extracted iodide was mainly not volatised by combustion of the resin and was converted to CuI. We conclude that the Cu-loaded bispicolylamine functionality has great potential for the intended remit and could even be married to other support matrices for future investigations, which it is hoped this work will stimulate.

Declaration of Competing Interest

The authors declare that they have no known competing financial interests or personal relationships that could have appeared to influence the work reported in this paper.

Acknowledgements

The authors wish to thank Mr Alex Riley (Dept. CBE), Mr Neil Bramall (Dept. Chemistry), Ms Heather Grievson (Dept. Chemistry) and Ms Elaine Frary (Dept. Chemistry) for technical assistance in analysis. We also gratefully thank Purolite® for their donation of MTS9850 resin.

Appendix A. Supplementary data

Supplementary data to this article can be found online at https://doi.org/10.1016/j.cej.2020.124647.

References

[1] F. Alam, R. Sarkar, H. Chowdhury, Nuclear power plants in emerging economies and human resource development: A review, 2nd International Conference on Energy and Power, 160 (2019) 3-10.
[2] M.K. Nasab, L.R. Motavalli, H.M. Hakimabad, Internal dosimetry of inhaled iodine-131, J. Environ. Radioact. 181 (2018) 62–69.
[3] E. Ostroumova, A. Rozhko, M. Hatch, K. Furukawa, O. Polyanskaya, R.J. McConnell, E. Nadyrov, S. Petrenko, G. Romanov, V. Yauseyenka, V. Drozdovitch, V. Minenko, A. Prokopovich, I. Savasteeva, L.B. Zablotska, K. Mabuchi, A.V. Brenner, Measures of Thyroid Function among Belarusian Children and Adolescents Exposed to Iodine-131 from the Accident at the Chernobyl Nuclear Plant, Environ. Health Perspect. 121 (2013) 865–871.
[4] Y.V. Zabaluev, Management of radionuclides from reprocessing plant gaseous effluents, IAEA Bull. 21 (1979) 23–31.
[5] Y.P. Zhirnov, M.I. Zhikharev, E.P. Efremov, R.S. Malankina, Behavior of molybdenum during evaporation of nitric-acid raffinates, At. Energ. 83 (1997) 848–850.
[6] J.V.I. Battle, T. Aono, J.E. Brown, A. Hosseini, J. Gamier-Laplace, T. Sazykina, F. Steenhuisen, P. Strand, The impact of the Fukushima nuclear accident on marine biota: Retrospective assessment of the first year and perspectives, Sci. Total Environ. 487 (2014) 143–153.
[7] J.M. Schofield, S.W. Swanton, B. Farahani, B.J. Myatt, T.G. Heath, S.E. Burrows, D. Holland, A. Moule, C.T. Brigden, I. Farnan, Experimental studies of the chemical durability of UK HLW and ILW glasses, AMEC Foster Wheeler, Didcot, 2016.
[8] R.T. Jubin, Airborne waste management technology applicable for use in reprocessing plants for control of iodine and other off-gas constituents, Oak Ridge National Laboratory, Tennessee, 1988.
[9] M. Gourani, A. Sadighzadeh, F. Mizani, Effect of impregnating materials in activated carbon on Iodine -131 (^{131}I) removal efficiency, Radiat. Prot. Environ. 37 (2014) 179–183.
[10] Z.J. Yan, Y. Yuan, Y.Y. Tian, D.M. Zhang, G.S. Zhu, Highly efficient enrichment of volatile iodine by charged porous aromatic frameworks with three sorption sites, Angewandte Chemie-International Edition 54 (2015) 12733–12737.
[11] F. Ren, Z.Q. Zhu, X. Qian, W.D. Liang, P. Mu, H.X. Sun, J.H. Liu, A. Li, Novel thiophene-bearing conjugated microporous polymer honeycomb-like porous spheres with ultrahigh iodine uptake, Chem. Commun. 52 (2016) 9797–9800.
[12] P.K. Sinha, K.B. Lal, J. Ahmed, Removal of radioiodine from liquid effluents, Waste Manage. 17 (1997) 33–37.
[13] X.Y. Zhang, P. Gu, X.Y. Li, G.H. Zhang, Efficient adsorption of radioactive iodide ion from simulated wastewater by nano Cu_2O/Cu modified activated carbon, Chem. Eng. J. 322 (2017) 129–139.
[14] D.N.T. Barton, T.J. Robshaw, O. Okusanya, D. Kim, S.E. Pepper, C.A. Sharrad, M.D. Ogden, Remediation of radioiodine using polyamine anion exchange resins, J. Ind. Eng. Chem. 78 (2019) 210–221.
[15] A. Meleshyn, U. Noseck, Asme, Radionuclide inventory of vitrified waste after spent nuclear fuel reprocessing at La Hague, 15th International Conference on Environmental Remediation and Radioactive Waste Management, Vol 1: Low/Intermediate-Level Radioactive Waste Management, Asme, 2013.
[16] T. Fukasawa, K. Funabashi, Y. Kondo, Influences of impurities on iodine removal efficiency of silver alumina adsorbent, Proceedings of the 24th DOE/NRC Nuclear Air Cleaning and Treatment Conference, Portland, Oregon, 1996.
[17] T.R. Thomas, B.A. Staples, L.P. Murphy, Development of Ag0Z for bulk ^{129}I removal from nuclear fuel reprocessing plants and PbX for ^{129}I storage, Nuclear air cleaning conference, Boston, Massachusetts, 1978.
[18] C. Decamp, S. Happel, Utilization of a mixed-bed column for the removal of iodine from radioactive process waste solutions, J. Radioanal. Nucl. Chem. 298 (2013) 763–767.
[19] T. Robshaw, S. Tukra, D.B. Hammond, G.J. Leggett, M.D. Ogden, Highly efficient fluoride extraction from simulant leachate of spent potlining via La-loaded chelating resin. An equilibrium study, J. Hazard. Mater. 361 (2019) 200–209.
[20] P. Outola, H. Leinonen, M. Ridell, J. Lehto, Acid/base and metal uptake properties of chelating and weak base resins, Solvent Extr. Ion Exch. 19 (2001) 743–756.
[21] A.L. Riley, S.E. Pepper, A.J. Canner, S.F. Brown, M.D. Ogden, Metal recovery from jarosite waste - A resin screening study, Sep. Sci. Technol. 53 (2018) 22–35.
[22] M.D. Ogden, E.M. Moon, A. Wilson, S.E. Pepper, Application of chelating weak base resin Dowex M4195 to the recovery of uranium from mixed sulfate/chloride media, Chem. Eng. J. 317 (2017) 80–89.
[23] K.-Y. Choi, H. Ryu, N.-D. Sung, M. Suh, Synthesis, properties, and X-ray structure of $[Cu(dpa)Cl_2]$ (dpa = di-(2-picolyl)amine), J. Chem. Crystallogr. 33 (2003) 947–950.
[24] W. Du, B.C. Pan, P.J. Jiang, Q.R. Zhang, W.M. Zhang, B.J. Pan, Q.J. Zhang, Q.X. Zhang, Selective sorption and preconcentration of tartaric acid using a copper (II)-bound polymeric ligand exchanger, Chem. Eng. J. 139 (2008) 63–68.
[25] G.J. Sutton, Some Studies in Inorganic Complexes. VII. Copper(II) with 2-Picolylamine, Aust. J. Chem. 13 (1960) 222–224.
[26] The Dow Chemical Company, DOWEX M4195. Chelating resin for copper, nickel, and cobalt processing, 2019, https://www.lenntech.com/Data-sheets/Dowex-M-4195-L.pdf.
[27] T.G. Fawcett, F. Needham, C. Crowder, S. Kabekkodu, Advanced materials analysis using the powder diffraction file,10th National Conference on X-ray Diffraction and ICDD Workshop, Shanghai, China, 2009.
[28] D. Kolodynska, W. Sofinska-Chmiel, E. Mendyk, Z. Hubicki, DOWEX M 4195 and LEWATIT (R) MonoPlus TP 220 in Heavy Metal Ions Removal from Acidic Streams, Sep. Sci. Technol. 49 (2014) 2003–2015.
[29] J. Spencer, J. Stevens, C. Perry, D.M. Murphy, An EPR Investigation of Binding Environments by N-Donor Chelating Exchange Resins for Cu Extraction from Aqueous Media, Inorg. Chem. 57 (2018) 10857–10866.
[30] R.R. Grinstead, Selective absorption of copper, nickel, cobalt and other transition-metal ions from sulfuric-acid-solutions with the chelating ion-exchange resin XFS 4195, Hydrometallurgy 12 (1984) 387–400.
[31] C.V. Diniz, F.M. Doyle, V.S.T. Ciminelli, Effect of pH on the absorption of selected heavy metal ions from concentrated chloride solutions by the chelating resin Dowex M4195, Sep. Sci. Technol. 37 (2002) 3169–3185.
[32] A. Wolowicz, Z. Hubicki, The use of the chelating resin of a new generation Lewatit MonoPlus TP-220 with the bis-picolylamine functional groups in the removal of selected metal ions from acidic solutions, Chem. Eng. J. 197 (2012) 493–508.
[33] P. Mao, Y. Liu, Y. Jiao, S.W. Chen, Y. Yang, Enhanced uptake of iodide on Ag/Cu_2O nanoparticles, Chemosphere 164 (2016) 396–403.
[34] E.J. Billo, Excel for Chemists: A Comprehensive Guide, 3 ed., John Wiley, Hoboken, New Jersey, 2004.
[35] S.E. Pepper, K.R. Whittle, L.M. Harwood, J. Cowell, T.S. Lee, M.D. Ogden, Cobalt and nickel uptake by silica-based extractants, Sep. Sci. Technol. 53 (2018) 1552–1562.
[36] A.M. James, S. Harding, T. Robshaw, N. Bramall, M.D. Ogden, R. Dawson, Selective Environmental Remediation of Strontium and Cesium Using Sulfonated Hyper-Cross-Linked Polymers (SHCPs), Appl. Mater. Interfaces 11 (2019) 22464–22473.
[37] S. Vasiliu, I. Bunia, S. Racovita, V. Neagu, Adsorption of cefotaxime sodium salt on polymer coated ion exchange resin microparticles: Kinetics, equilibrium and thermodynamic studies, Carbohydr. Polym. 85 (2011) 376–387.
[38] Y.L. Nie, C. Hu, C.P. Kong, Enhanced fluoride adsorption using Al (III) modified calcium hydroxyapatite, J. Hazard. Mater. 233 (2012) 194–199.
[39] K. Vijayaraghavan, T.V.N. Padmesh, K. Palanivelu, M. Velan, Biosorption of nickel (II) ions onto Sargassum wightii: Application of two-parameter and three-parameter isotherm models, J. Hazard. Mater. 133 (2006) 304–308.
[40] M.S. Refat, H. Al Didamony, K.M. Abou El-Nour, L. El-Zayat, Synthesis and spectroscopic characterization on the tri-iodide charge transfer complex resulted from the interaction between morpholine as donor and iodine sigma-acceptor, J. Saudi Chem. Soc. 14 (2010) 323–330.
[41] A.A. Fakhroo, H.S. Bazzi, A. Mostafa, L. Shahada, Synthesis, spectroscopic and thermal structural investigations of the charge-transfer complexes formed in the reaction of 1-methylpiperidine with sigma- and pi-acceptors, Spectrochim. Acta Part A-Mol. Biomolecular Spectrosc. 75 (2010) 134–141.
[42] N. Miyajima, T. Akatsu, T. Ikoma, O. Ito, B. Rand, Y. Tanabe, E. Yasuda, A role of charge-transfer complex with iodine in the modification of coal tar pitch, Carbon 38 (2000) 1831–1838.
[43] M.H. Zeng, Q.X. Wang, Y.X. Tan, S. Hu, H.X. Zhao, L.S. Long, M. Kurmoo, Rigid Pillars and Double Walls in a Porous Metal-Organic Framework: Single-Crystal to Single-Crystal, Controlled Uptake and Release of Iodine and Electrical Conductivity, J. Am. Chem. Soc. 132 (2010) 2561–2563.

[44] G.L. Hatch, J.L. Lambert, L.R. Fina, Some properties of the quaternary ammonium anion-exchange resin-triiodide disinfectant for water, Ind. Eng. Chem. Prod. Res. Dev. 19 (1980) 259–263.
[45] J.L. Lambert, G.T. Fina, L.R. Fina, Preparation and properties of triiodide-quaternary, pentaiodide-quaternary, and heptaiodide-quaternary ammonium strong base anion-exchange resin disinfectants, Ind. Eng. Chem. Prod. Res. Dev. 19 (1980) 256–258.
[46] I. Sanemasa, M. Yoshida, A. Abe, Uptake of iodine and bromine by ion-exchange resins in aqueous solution, Anal. Sci. 24 (2008) 921–924.
[47] R. Peng, M. Li, D. Li, Copper(I) halides: A versatile family in coordination chemistry and crystal engineering, Coord. Chem. Rev. 254 (2010) 1–18.
[48] G.A. Senchyk, A.B. Lysenko, K.V. Domasevitch, O. Erhart, S. Henfling, H. Krautscheid, E.B. Rusanov, K.W. Kramer, S. Decurtins, S.X. Liu, Exploration of a Variety of Copper Molybdate Coordination Hybrids Based on a Flexible Bis(1,2,4-triazole) Ligand: A Look through the Composition-Space Diagram, Inorg. Chem. 56 (2017) 12952–12966.
[49] T.J. Robshaw, K. Bonser, G. Coxhill, R. Dawson, M.D. Ogden, Development of a combined leaching and ion-exchange system for valorisation of spent potlining waste, Waste and Biomass Valorization, in-press (2020).
[50] M.H. Calero, F. Blázquez, G. Tenorio, G. Martín-Lara, M.A, Study of Cr (III) biosorption in a fixed-bed column, J. Hazard. Mater. 171 (2009) 886–893.
[51] T.J. Robshaw, R. Dawson, K. Bonser, M.D. Ogden, Towards the implementation of an ion-exchange system for recovery of fluoride commodity chemicals, Kinet. Dyn. Stud. Chem. Eng. J. 367 (2019) 149–159.
[52] K.H. Chu, Fixed bed sorption: Setting the record straight on the Bohart-Adams and Thomas models, J. Hazard. Mater. 177 (2010) 1006–1012.
[53] J. Blumberger, L. Bernasconi, I. Tavernelli, R. Vuilleumier, M. Sprik, Electronic structure and solvation of copper and silver ions: A theoretical picture of a model aqueous redox reaction, J. Am. Chem. Soc. 126 (2004) 3928–3938.
[54] G.A. Bowmaker, J.V. Hanna, C. Pakawatchai, B.W. Skelton, Y. Thanyasirikul, A.H. White, Crystal Structures and Vibrational Spectroscopy of Copper(I) Thiourea Complexes, Inorg. Chem. 48 (2009) 350–368.
[55] K.R. Mahmoud, M.S. Refat, T. Sharshar, A.M.A. Adam, E.S.A. Manaaa, Synthesis of amino acid iodine charge transfer complexes in situ methanolic medium: Chemical and physical investigations, J. Mol. Liq. 222 (2016) 1061–1067.
[56] J. Milne, A raman-spectroscopic study of the effect of ion-pairing on the structure of the triiodide and tribromide ions, Spectrochimica Acta Part A-Molecular and Biomolecular Spectroscopy 48 (1992) 533–542.
[57] I. Jerman, V. Jovanovski, A.S. Vuk, S.B. Hocevar, M. Gaberscek, A. Jesih, B. Orel, Ionic conductivity, infrared and Raman spectroscopic studies of 1-methyl-3-propylimidazolium iodide ionic liquid with added iodine, Electrochim. Acta 53 (2008) 2281–2288.
[58] S. Mondal, A. Gupta, B.K. Shaw, S.K. Saha, Photo-induced conductivity in 2,6-diaminopyridine functionalized graphene oxide containing Eu^{2+} for optoelectronic applications, Opt. Mater. 73 (2017) 555–562.
[59] M.C. Biesinger, L.W.M. Lau, A.R. Gerson, R.S.C. Smart, Resolving surface chemical states in XPS analysis of first row transition metals, oxides and hydroxides: Sc, Ti, V, Cu and Zn, Applied Surface Science 257 (2010) 887–898.
[60] I.L. Malaestean, V.C. Kravtsov, J. Lipkowski, E. Cariati, S. Righetto, D. Marinotto, A. Forni, M.S. Fonari, Partial in Situ Reduction of Copper(II) Resulting in One-Pot Formation of 2D Neutral and 3D Cationic Copper(I) Iodide-Pyrazine Coordination Polymers: Structure and Emissive Properties, Inorg. Chem. 56 (2017) 5141–5151.
[61] S.K. Guchhait, A.L. Chandgude, G. Priyadarshani, $CuSO_4$-Glucose for in Situ Generation of Controlled Cu(I)-Cu(II) Bicatalysts: Multicomponent Reaction of Heterocyclic Azine and Aldehyde with Alkyne, and Cycloisomerization toward Synthesis of N-Fused Imidazoles, J. Org. Chem. 77 (2012) 4438–4444.
[62] A. Chilkoti, B.D. Ratner, X-ray photoelectron-spectroscopy of iodine-doped non-conjugated polymers, Chem. Mater. 5 (1993) 786–792.
[63] C. Das, M. Wussler, T. Hellmann, T. Mayer, W. Jaegermann, In situ XPS study of the surface chemistry of MAPI solar cells under operating conditions in vacuum, PCCP 20 (2018) 17180–17187.
[64] G.A. Bowmaker, C. Di Nicola, C. Pettinari, B.W. Skelton, N. Somers, A.H. White, Mechanochemical synthesis in copper(II) halide/pyridine systems: single crystal X-ray diffraction and IR spectroscopic studies, Dalton Trans. 40 (2011) 5102–5115.
[65] R.E. Buckles, J.P. Yuk, A.I. Popov, The stability of the tetramethylammonium polyiodides in ethylene chloride, J. Am. Chem. Soc. 74 (1952) 4379–4381.
[66] K.S. Tan, A.C. Grimsdale, R. Yazami, A room-temperature refuelable lithium, iodine and air battery, Sci. Rep. 7 (2017).
[67] H. Zhou, B. Zhao, C. Fu, Z.Q. Wu, C.G. Wang, Y. Ding, B.H. Han, A.G. Hu, Synthesis of Conjugated Microporous Polymers through Cationic Cyclization Polymerization, Macromolecules 52 (2019) 3935–3941.
[68] J.L. Wang, Z. Wan, Treatment and disposal of spent radioactive ion-exchange resins produced in the nuclear industry, Prog. Nucl. Energy 78 (2015) 47–55.
[69] V. Luca, H.L. Bianchi, A.C. Manzini, Cation immobilization in pyrolyzed simulated spent ion exchange resins, J. Nucl. Mater. 424 (2012) 1–11.
[70] H.C. Yang, M.W. Lee, H.S. Hwang, J.K. Moon, D.Y. Chung, Study on thermal decomposition and oxidation kinetics of cation exchange resins using non-isothermal TG analysis, J. Therm. Anal. Calorim. 118 (2014) 1073–1083.